Preparation and Crystallographic Characterization of a New Endohedral, $Lu_3N@C_{80}\cdot 5(o\text{-xylene})$, and Comparison with $Sc_3N@C_{80}\cdot 5(o\text{-xylene})$

Steve Stevenson,[b] Hon Man Lee,[a] Marilyn M. Olmstead,[a] Carrie Kozikowski,[b] Paige Stevenson,[b] and Alan L. Balch*[a]

Abstract: The trimetallic nitride template (TNT) approach has been successfully utilized to prepare the new endohedral $Lu_3N@C_{80}$. Well-ordered crystals of $Lu_3N@C_{80}\cdot 5(o\text{-xylene})$ and $Sc_3N@C_{80}\cdot 5(o\text{-xylene})$ form upon cooling of *o*-xylene solutions of these endohedrals and they are isomorphous. Although the positions of the fullerene cage (which is fully ordered and located at a crystallographic center of symmetry) and the *o*-xylene molecules are nearly identical in these two structures, the positioning of the metal ions in the two crystals differ in significant ways. However, the expected difference in sizes of lutetium and scandium does not affect the dimensions of the C_{80} cage. Nevertheless, the positions of the metal atoms do produce a slight outward dislocation of the immediately adjacent carbon atoms.

Keywords: endohedrals · fullerenes · lutetium · scandium · structure elucidation · X-ray diffraction

Introduction

Endohedral fullerenes, that is, fullerenes with atoms mechanically trapped in their interior, have been known since the beginnings of fullerene chemistry.[1] However, acquisition of sufficient quantities of these novel molecules for chemical and physical study has been limited by the low yields in which most endohedrals are produced. Moreover, some endohedrals display low solubility in organic solvents and sensitivity toward dioxygen. Despite these limitations, a substantial number of endohedral species have been detected, and in a number of cases the endohedrals have been purified by chromatography as noted in recent reviews.[2–4]

Recently the novel endohedral $Sc_3N@C_{80}$ has been prepared in remarkably high yield and purity.[5, 6] Endohedral $Sc_3N@C_{80}$ contains a planar tetraatomic Sc_3N unit confined within an C_{80} cage with I_h symmetry. This is one of seven isomeric structures for the C_{80} cage that fulfill the isolated pentagon rule.[7] $Sc_3N@C_{80}$ is produced by modifying the normal Krätschmer–Huffman arc fullerene preparation through the use of a dynamic atmosphere that contains dinitrogen in addition to the usual helium- and scandium-oxide-doped graphite rods. This process, the trimetallic nitride template (TNT) method, produces $Sc_3N@C_{80}$ in quantities which exceed that of C_{84}, which is generally the third most abundant fullerene after C_{60} and C_{70}. As a result, macroscopic quantities of $Sc_3N@C_{80}$ are now available for chemical and physical characterization. Physical studies conduced so far on $Sc_3N@C_{80}$ include characterization by NMR (^{13}C, ^{14}N, and ^{45}Sc) spectroscopy, UV-visible absorption spectroscopy, and single-crystal X-ray diffraction.[5] The NMR results indicate that the Sc_3N portion freely rotates with regard to the C_{80} cage in solution at room temperature. The entire neutral endohedral is viewed as composed of a central N^{3-} unit surrounded by three Sc^{3+} ions and enclosed within a C_{80} cage bearing a 6− charge. Density functional calculations support this sort of charge distribution for $Sc_3N@C_{80}$ and show that the barrier for rotation of the Sc_3N unit within the C_{80} cage is small.[8] Chemical studies have shown that $Sc_3N@C_{80}$ undergoes Diels–Alder addition to a 5:6 ring junction, rather that at a 6:6 ring junction which is generally the prefered site of addition in C_{60} and C_{70}.[9] The structure of the resulting product, $Sc_3N@C_{80}C_{10}H_{10}O_2$, has been determined by single-crystal X-ray diffraction.[10]

The TNT process with scandium-oxide-doped graphite rods also produces smaller quantities of two other endohedrals: $Sc_3N@C_{78}$, with the Sc_3N unit located at the waist of a fullerene cage with D_{3h} symmetry,[11] and $Sc_3N@C_{68}$, which contains a fullerene cage that cannot obey the isolated pentagon rule.[12] By employing graphite rods doped with rare earth metal oxides, it has been possible to prepare other TNT fullerenes including $Er_3N@C_{80}$ and $Y_3N@C_{80}$.[6] Utiliza-

[a] Prof. Dr. A. L. Balch, Dr. H. M. Lee, Dr. M. M. Olmstead
Department of Chemistry, University of California
Davis, California 95616 (USA)
Fax: (+1) 530-752-8995
E-mail: albalch@ucdavis.edu

[b] Dr. S. Stevenson, Dr. C. Kozikowski, Dr. P. Stevenson
Luna Nanomaterials, 2851 Commerce Street
Blacksburg, VA 24060 (USA)

  0947-6539/02/0819-4528 $ 20.00+.50/0

tion of graphite rods doped with a mixture of scandium oxide and a rare earth metal oxide has led to the formation of the mixed metal endohedrals: $Sc_2MN@C_{80}$ and $ScM_2N@C_{80}$ in which M = Er, Ho, Y, La, Gd, and Tm.[6] Of these, $ErSc_2N@C_{80}$ has been isolated and purified.[13] Its structure has been determined by single-crystal X-ray diffraction. The Er^{3+} fluorescence from $Er_nSc_{3-n}N@C_{80}$ ($n = 1, 2,$or 3) has been interpreted in terms of the structures of these endohedrals.[14] The electron affinities of $Er_nSc_{3-n}N@C_{80}$ ($n = 0, 1, 2,$or 3) have been measured by a mass spectrometric procedure.[15]

Here we report the formation, purification and isolation of a new rare earth endohedral, $Lu_3N@C_{80}$. Since the ionic radius of Lu^{3+} (0.848 Å) is larger than that of Sc^{3+} (0.68 Å),[16] the structures of $Lu_3N@C_{80}$ and $Sc_3N@C_{80}$ have been examined by single-crystal X-ray diffraction to assess the effects of accommodating the presumably larger rare earth ions. A theoretical study that compared $La_3N@C_{80}$ to $Sc_3N@C_{80}$ suggested that the La_3N portion in the former might adopt a pyramidal rather than planar arrangement.[17] Although La^{3+} (ionic radius 1.061 Å) is even larger than Lu^{3+}, the size discrepancy between Lu^{3+} and Sc^{3+} is significant enough to expect some degree of structural variation between $Lu_3N@C_{80}$ and $Sc_3N@C_{80}$.

Results

Synthesis, isolation, and characterization of $Lu_3N@C_{80}$: Following the usual TNT procedure, arc-burning of graphite rods packed with 5 % Lu_2O_3/95 % graphite powder (with cobalt(II) oxide as a catalyst) in a Krätschmer–Huffman fullerene generator under dynamic flow of helium and dinitrogen produced black soot. This soot contains primarily amorphous carbon with small amounts of fullerene species: empty-cage fullerenes (C_{60}, C_{70}, C_{84}), classical metallofullerenes $Lu_2@C_{82}$, as well as the newly discovered TNT metallofullerene $Lu_3N@C_{80}$. Fullerene-containing extracts can be readily obtained by extracting the soot with organic solvents, such as carbon disulfide, aromatic hydrocarbons, and polar solvents, such as *N*,*N*-dimethylformamide. Characterization of these TNT fullerene extracts was done by mass spectrometry. The negative ion, desorption chemical ionization mass spectra for carbon disulfide extracts of lutetium and scandium soot are compared in Figure 1.

$Lu_3N@C_{80}$ was isolated from the raw soot and purified through two stages of high-pressure liquid chromatography (HPLC) with *o*-xylene as solvent. The fullerene extracts in *o*-xylene were initially separated through the use of a pentabromobenzyl (PBB) column to remove the empty-cage fullerenes (particularly C_{60} and C_{70}). The second stage of HPLC involved the injection of the enriched PBB fraction into a BuckyPrep column (Phenomenex, 10 × 250 mm). The final HPLC traces as well as their corresponding mass spectral data are shown in Figure 2. From six packed graphite rods (0.5 × 15.5 cm), 150 mg of soluble extract was obtained and 5 mg of purified $Lu_3N@C_{80}$ was recovered.

Figure 3 compares the UV-visible absorption spectra of $Lu_3N@C_{80}$ and $Sc_3N@C_{80}$. The differences seen show that the spectra are affected by the contents of the cage and are not simply a reflection of the presence of C_{80} cage with icosahedral symmetry.

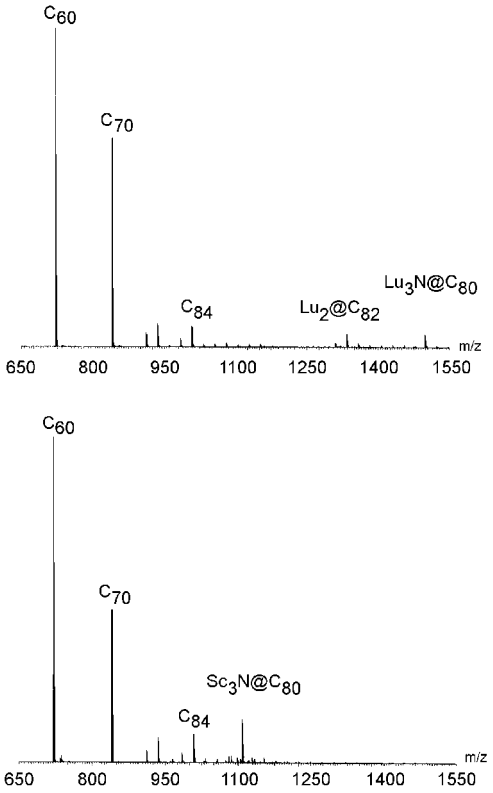

Figure 1. Negative ion mass spectra of lutetium and scandium fullerene extracts.

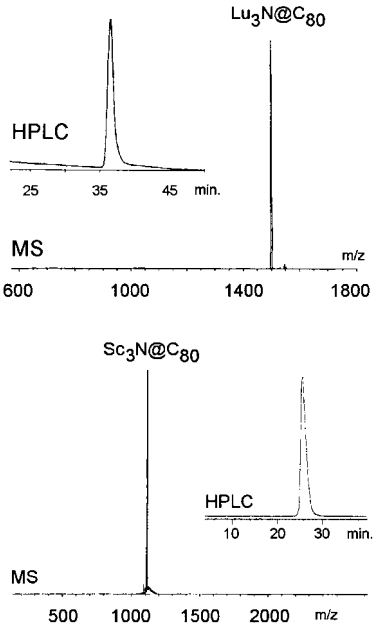

Figure 2. HPLC and mass spectra of the purified samples of $Lu_3N@C_{80}$ and $Sc_3N@C_{80}$ used in this work.

Crystallization and structural analysis of $Lu_3N@C_{80}\cdot 5$(*o*-xylene) and $Sc_3N@C_{80}\cdot 5$(*o*-xylene) at 90 K: During the processing of extracts of $Sc_3N@C_{80}$ in *o*-xylene, we noticed that crystalline material formed when hot, concentrated

  0947-6539/02/0819-4529 $ 20.00+.50/0

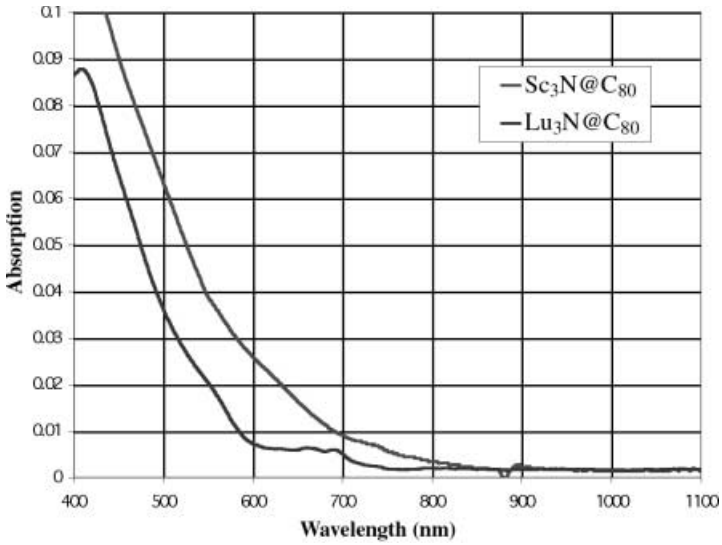

Figure 3. UV-visible spectra of $Lu_3N@C_{80}$ and $Sc_3N@C_{80}$.

solutions of the extract were allowed to cool. These crystals along with similar crystals from the $Lu_3N@C_{80}$ extract were examined by single-crystal X-ray diffraction at low temperature (90 K).

As seen from the crystallographic data (Table 1), crystals of $Lu_3N@C_{80}\cdot 5(o\text{-xylene})$ and $Sc_3N@C_{80}\cdot 5(o\text{-xylene})$ are isomorphous. Table 2 presents a comparison of selected interatomic distances and angles in the two structures. Figure 4 shows a view of the unit cell for $Lu_3N@C_{80}\cdot 5(o\text{-xylene})$. (That of $Sc_3N@C_{80}\cdot 5(o\text{-xylene})$ is identical.) In this drawing the positions of the metal atoms, which are disordered, are not shown. The nitrogen atom of the $Lu_3N@C_{80}$ molecule sits at a crystallographic inversion center. Consequently the fullerene cage, which is fully ordered, also is situated at a crystallographic center of symmetry. There are three different *o*-xylene molecules in the asymmetric unit. Two of these, *o*-xylene-1, which contains C49 – C56, and *o*-xylene-2, which contains C57 – C64, make face-to-face contact with the adjacent fullerene cage. The distance from the plane of the *o*-xylene molecules to the nearest fullerene carbon atom (C11) is 3.223(10) Å for *o*-xylene-1 and 3.110(10) Å to C22 for *o*-xylene-2. The shortest nonbonded C···C distance between *o*-xylene-1 and the cage is 3.343(10) Å (for C11···C49) and between *o*-xylene 2 and the other cage it is 3.135(10) Å (for C57···C22D). The third *o*-xylene molecule (*o*-xylene-3, which contains C41 – C48) is situated at a center of symmetry and is disordered over two alternate orientations. There is no close face-to-face contact of *o*-xylene-3 with any of the nearby fullerene cages.

Table 1. Crystallographic data for $Lu_3N@C_{80}\cdot 5(o\text{-xylene})$ and $Sc_3N@C_{80}\cdot 5(o\text{-xylene})$.

	$Lu_3N@C_{80}\cdot 5(o\text{-xylene})$	$Sc_3N@C_{80}\cdot 5(o\text{-xylene})$
formula	$C_{120}H_{50}NLu_3$	$C_{120}H_{50}NSc_3$
M_r	2030.52	1640.49
a [Å]	10.9873(19)	10.9735(9)
b [Å]	11.0872(19)	11.1665(9)
c [Å]	14.356(3)	14.3101(11)
α [°]	82.747(3)	82.716(2)
β [°]	84.111(4)	84.728(2)
γ [°]	80.741(3)	80.395(2)
V [Å^3]	1706.2(5)	1710.5(2)
Z	1	1
crystal system	triclinic	triclinic
space group	$P\bar{1}$	$P\bar{1}$
T [K]	90(2)	90(2)
λ [Å]	0.71073	0.71073
ρ [g cm^{-3}]	1.976	1.593
μ [mm^{-1}]	4.374	0.357
max/min transmission	0.45/0.34	0.92/0.89
data/restraints/parameters	6689/0/656	6737/0/611
$R1$ (obsd data)[a]	0.060	0.080
$wR2$ (all data, F^2 refinement)[b]	0.183	0.244

[a] $R1=\Sigma||F_o|-|F_c||/\Sigma|F_o|$, observed data $[I>4\sigma(I_o)]$. [b] $wR2=[\Sigma[w(F_o^2-F_c^2)^2]/\Sigma[w(F_o^2)^2]]^{1/2}$, all data.

Table 2. Selected bond lengths [Å] and angles [°] for $Lu_3N@C_{80}$ and $Sc_3N@C_{80}$.

	$Lu_3N@C_{80}$	$Sc_3N@C_{80}$
M1–N1	2.001(3)	1.9931(14)
M2–N1	2.0819(8)	2.0323(16)
M3–N1	2.0592(10)	2.0526(14)
M1B–N1	1.980(6)	
M2B–N1	2.0083(16)	1.981(10)
M3B–N1	2.0728(18)	
M1C–N1	2.00(2)	
M2C–N1	2.003(9)	
M3C–N1	2.063(11)	
M1D–N1	2.07(2)	
M3D–N1	2.07(3)	
M1···M2	3.554(3)	3.498(2)
M1···M3	3.543(3)	3.490(2)
M2···M3	3.528(1)	3.510(2)
M1B···M2B	3.469(7)	3.421(10)[a]
M1B···M3B	3.500(8)	
M2B···M3B	3.530(3)	3.448(10)[b]
M1C···M2C	3.51(3)	
M1C···M3C	3.49(3)	
M2C···M3C	3.50(2)	
M1D···M2C	3.52(3)	
M1D···M3D	3.54(4)	
M2C···M3D	3.57(3)	
M1–C8	2.220(7)	2.205(4)
M2–C21	2.112(7)	2.147(4)
M3–C28	2.165(7)	2.145(4)C29
M1B–C25	2.219(9)	
M2B–C32	2.147(6)	2.134(10)
M3B–C11	2.142(7)	
M1C–C27	2.15(2)	
M2C–C24	2.115(12)	
M3C–C31	2.058(13)	
M1D–C1	2.07(2)	
M3D–C14	2.04(3)	
M1-N1-M2	121.00(11)	120.70(7)
M1-N1-M3	121.51(11)	119.21(6)
M2-N1-M3	123.97(15)	118.47(7)
M1B-N1-M2B	120.8(3)	118.8(3)[a]
M1B-N1-M3B	119.4(3)	
M2B-N1-M3B	119.74(10)	117.5(3)[b]
M1C-N1-M2C	122.8(9)	
M1C-N1-M3C	118.3(9)	
M2C-N1-M3C	118.6(7)	
M1D-N1-M2C	119.4(8)	
M1D-N1-M3D	117.6(11)	
M2C-N1-M3D	122.3(9)	

[a] Distance or angle to Sc1. [b] Distance or angle to Sc3.

Although the positions of the fullerene cage and the *o*-xylene molecules are nearly identical in both $Lu_3N@C_{80}\cdot 5(o$-

0947-6539/02/0819-4530 $ 20.00+.50/0 *Chem. Eur. J.* **2002**, *8*, No. 19

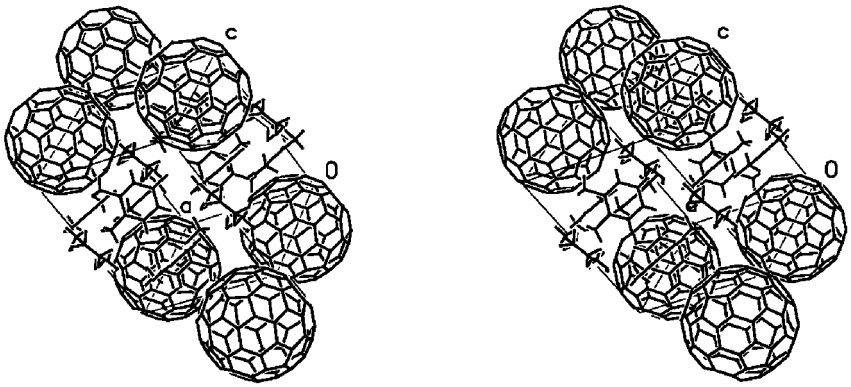

Figure 4. A stereoview of the unit cell for $Lu_3N@C_{80}\cdot 5$(*o*-xylene). For clarity the positions of the metal atoms and the nitrogen atom are not shown.

xylene) and $Sc_3N@C_{80}\cdot 5$(*o*-xylene), the positioning of the metal ions within the carbon cages in the two crystals differ in significant ways. The triangular M_3 unit cannot have a center of symmetry, and these portions of the solids are disordered. Figure 5A shows a drawing of the entire fully ordered C_{80} cage portion of $Sc_3N@C_{80}$ with 30% thermal contours for the carbon atoms. Figure 5B shows the positions of the scandium and nitrogen atoms (using 30% thermal contours) within the cage. Here the locations of the individual metal atoms in $Sc_3N@C_{80}$ are shown, but there are additional metal atom positions generated by the crystallographic center of inversion (for the sake of clarity these are omitted).

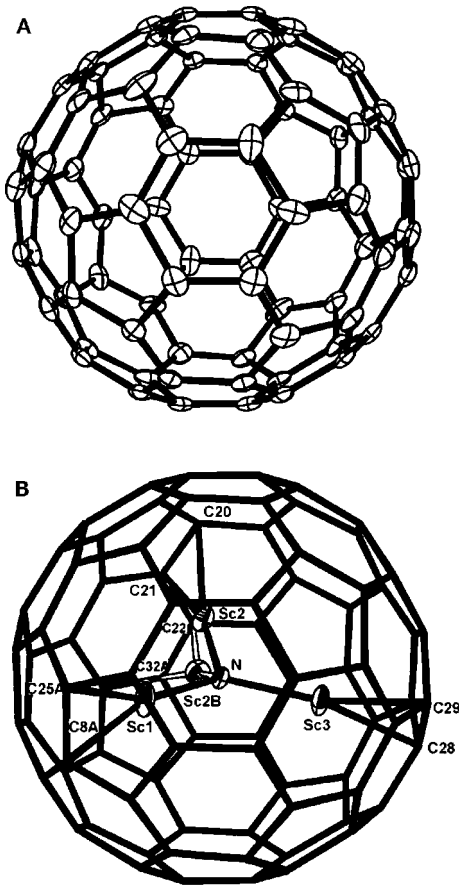

Figure 5. A) The C_{80} cage in $Sc_3N@C_{80}$ with 30% thermal contours without the Sc_3N unit. B) Positions of the Sc_3N units within $Sc_3N@C_{80}$. The C_{80} cage is shown as simple lines with 30% thermal contours for Sc_3N the units. The locations of individual groups of metal atoms are shown, but there are additional sets of metal atom positions generated by the presence of the center of inversion which are not shown.

Figure 6 shows similar information for $Lu_3N@C_{80}$. Figure 6A shows a drawing of the C_{80} cage with 30% thermal contours for the carbon atoms, whereas Figure 6B shows the position of the nitrogen atom and the major positions of the lutitium atoms (using 30% thermal contours) within that cage. Figure 6C shows the minor positions of the lutitium atoms (using 30% thermal contours) within that cage. There is an additional set of metal atom positions generated by the center of inversion, but for clarity this set is not shown. However, Figure 7 shows stereo views of $Lu_3N@C_{80}$ and $Sc_3N@C_{80}$ in which all of the metal atom positions, including those generated by the enter of symmetry, are shown.

The arrangement of metal atoms is considerably simpler for $Sc_3N@C_{80}$ than it is for $Lu_3N@C_{80}$. In $Sc_3N@C_{80}$ the principle metal atom sites involve Sc1, Sc2, and Sc3 with site occupancies of 0.5, 0.5, and 0.407(2), respectively. The larger site occupances of Sc(1) and Sc(2) occur because these sites combine with an alternative site, Sc2B with a site occupancy of 0.093(2), which forms a second Sc_3 triangle. The Sc–N distances span the narrow range 1.981(10) – 2.0526(14) Å. For comparison, the Sc–N distances in the well-ordered endohedral addition product $Sc_3N@C_{80}C_{10}H_{10}O_2$ range from 2.020(3) – 2.032(3) Å,[10] and the Sc–N distances in $ErSc_2N@C_{80}$ are 1.966(12) and 2.011(19) Å.[13] The Sc-N-Sc angles in $Sc_3N@C_{80}$ fall in the narrow range from 117.5(3) to 120.70(7)°, and the Sc_3N units are nearly planar.

In $Lu_3N@C_{80}$ there are four orientations of the Lu_3 unit within the fullerene as seen in Figure 6B and C. The principal site for this group involves Lu1, Lu2, and Lu3 with equal sites occupancies of 0.2986(10). An alternate location with a lower population involves the atoms Lu1B, Lu2B, and Lu3B with equal site occupancies of 0.1714(10). A third, minor orientation involves the atoms Lu1C, Lu2C, and Lu3C with occupancies of 0.0209(8), 0.03, and 0.0209(8), respectively. There are two other metal atoms sites, Lu1D and Lu3D with equal site occupancies of 0.00091(8). Sites Lu1D and Lu3D combine with added occupancy of site Lu2C to form a fourth orientation of the Lu_3 group. Each of these four orientations is converted into a second orientation by the center of symmetry. Thus there are 22 sites within the C_{80} cage that are populated with some fraction of a Lu atom in the crystal at 90 K.

All four of the resulting Lu_3N groups are nearly planar with Lu-N-Lu angles that range from 117.6(11) – 123.97(15)°. The Lu–N distances range from 1.980(6) – 2.0819(8) Å. Notice that the Sc–N distances in $Sc_3N@C_{80}$ fell in a similar range, 1.981(10) – 2.0526(14) Å. Consequently despite the larger

  0947-6539/02/0819-4531 $ 20.00+.50/0

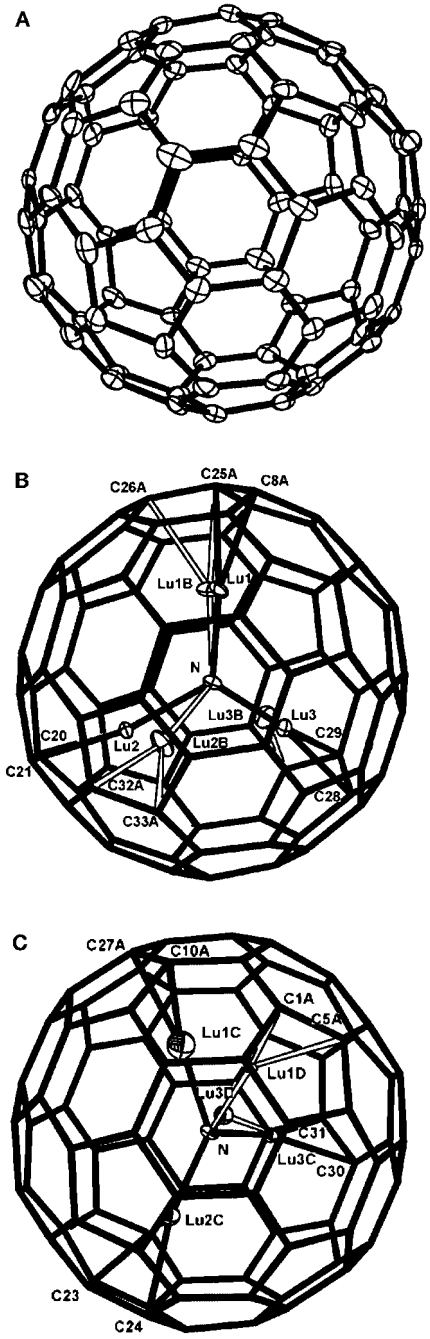

Figure 6. A) The C_{80} cage in $Lu_3N@C_{80}$ with 30% thermal contours, but without the Lu_3N unit. B) Positions of the major two Lu_3N units (Lu1 – Lu3 with 0.2986(10) occupancy; Lu1B – Lu3B with 0.1714(10) occupancy) within $Lu_3N@C_{80}$. C) Positions of the minor Lu_3N units (Lu1C – Lu3C with 0.0209(8) occupancy; Lu1D, Lu2C, Lu3D with 0.0091(8) occupancy) within $Lu_3N@C_{80}$. The C_{80} cage is shown as simple lines with 30% thermal contours for Lu_3N the units. There are additional sets of metal atom positions generated by the presence of the center of inversion which are not shown.

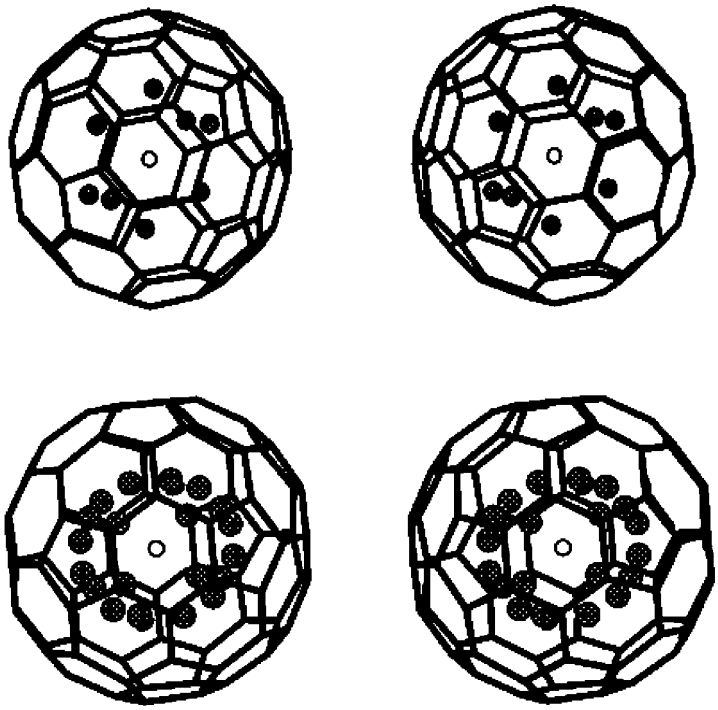

Figure 7. Stereo views of $Sc_3N@C_{80}$ (top) and $Lu_3N@C_{80}$ (bottom). All of the metal atom positions, including those generated by the center of symmetry, are shown.

ionic radius expected for lutetium, this factor does not appear to lengthen the Lu–N bonds, and the Lu–N and Sc–N distances are surprisingly similar in the two structures reported here.

Also the difference in expected sizes of lutetium and scandium does not effect the dimensions of the C_{80} cage. In the first place the unit cell volume for $Lu_3N@C_{80}$ is slightly smaller than that of the isomorphous $Sc_3N@C_{80}$. Additionally, the average C–C bond lengths at the 6:6 and 6:5 ring junctions are similar in the two structures. In $Sc_3N@C_{80}$ the average C–C bond length at the 6:6 ring junctions is 1.417(6) Å, and that at the 6:5 ring junctions is slightly larger, 1.449(6) Å. These figures are similar to those found in $Sc_3N@C_{80}C_{10}H_{10}O_2$, in which the average C–C bond lengths (excluding those at the site of addend attachment) are 1.421(18) Å at the 6:6 ring junctions and 1.437(15) Å at the 6:5 ring junctions. In $Lu_3N@C_{80}$ the average C–C bond length at the 6:6 ring junctions is 1.427(10) Å, and that at the 6:5 ring junctions is 1.438(10) Å.

The metal atoms within the C_{80} cages are positioned at 90 K so that they reside close to a single carbon atom. The distance from Sc or Lu to the nearest carbon atoms are given in Table 2. For the major sites (for which the parameters are most accurate), the Sc–C distances range from 2.145(4) – 2.205(4) Å. The Lu–C distances span a similar range, 2.112(7) – 2.220(7) Å.

The positions of the metal atoms do produce a slight outward projection of the immediately adjacent carbon atoms. This is best seen in Figure 8, which shows the non-bonded C···N distances for each of the different carbon atoms in the fullerene for both $Sc_3N@C_{80}$ and $Lu_3N@C_{80}$. Since these fullerene cages sit on sites of inversion symmetry, the nitrogen atom is precisely located at the center of each cage. Consequently, the C···N distances reflect subtle variations in the cage geometry. Since the structures are disordered, the effect on lengthening the C···N distances is greatest for those sites at which the fractional occupancy of the metal atom is greatest. As Figure 8 shows, the

  0947-6539/02/0819-4532 $ 20.00+.50/0 *Chem. Eur. J.* **2002**, *8*, No. 19

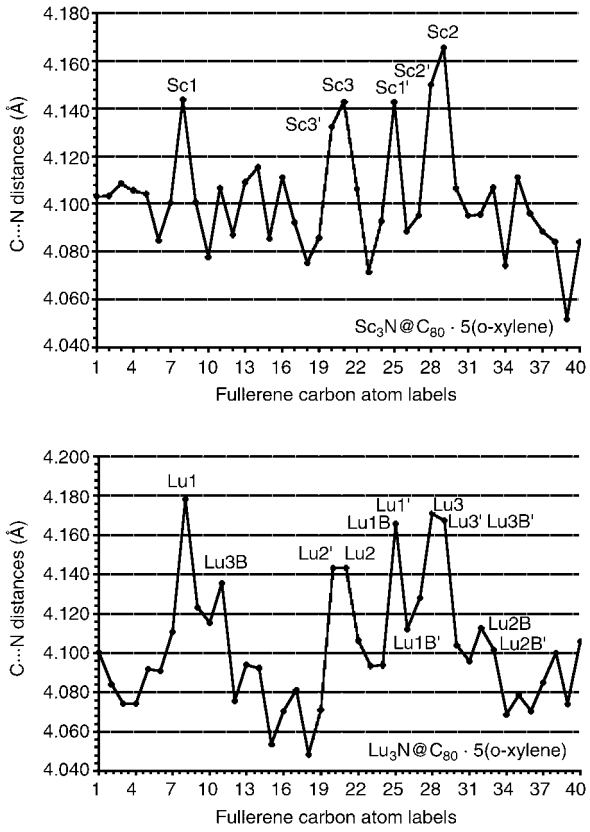

Figure 8. The nonbonded C···N distances for each of the different fullerene carbon atoms in $Sc_3N@C_{80}$ and $Lu_3N@C_{80}$. The carbon atoms nearest and next nearest to the predominant metal sites are labeled with the primes indicating the next nearest carbon atoms.

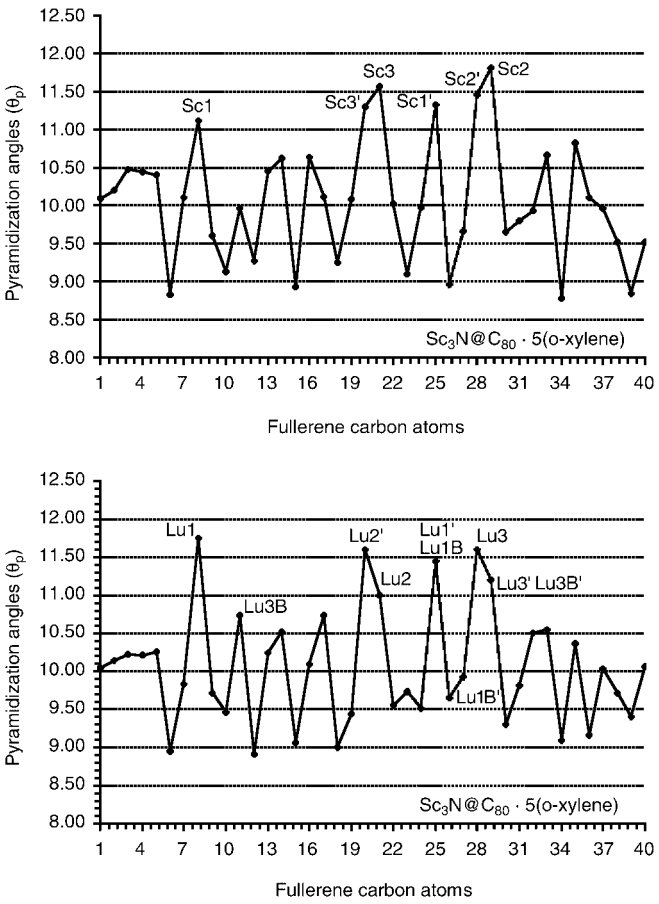

Figure 9. A plot of the pyramidazation angles (θ_p) for each of the different fullerene carbon atoms in $Sc_3N@C_{80}$ and $Lu_3N@C_{80}$. The carbon atoms nearest and next nearest to the predominant metal sites are labeled with the primes indicating the next nearest carbon atoms.

C···N distances are greatest for those carbon atoms that are closest to the metal atoms sites.

The distortion of the fullerene surface can also be seen by observing the pyramidalization angles (θp) for each fullerene carbon.[18] The relevant data for $Lu_3N@C_{80}$ and $Sc_3N@C_{80}$ are shown in Figure 9. (For comparison, the θp values of graphite and C_{60} are 0° and 11.6°, respectively.) The pyramidalization angles are greatest for those carbon atoms that are nearest the Sc or Lu atoms inside the fullerene cages. Similar data regarding the pyramidalization angles have been reported earlier for $Sc_3N@C_{80}C_{10}H_{10}O_2$.[11] The plots of the pyramidalization angles seen in Figure 9 closely parallel the plots of the C···N distances seen in Figure 8.

The crystal sturucture of $Sc_3N@C_{80}\cdot 5$(*o*-xylene) at 200 K: A different crystal was selected for this experiment. Data were collected as before, first at 200 K and then at 90 K without removing the crystal from the cold stream. The structure at 90 K proved to be identical, even with respect to the Sc disorder, to that collected on the previous crystal: $R1 = 0.072$ for 4329 $F_o > 4(F_o)$ and 637 parameters. The data collected at 200 K did not yield an ordered structure. The crystal system was still triclinic. The unit cell volume at 200 K was 2.4% larger, and all unit cell dimensions were increased. Although the high-temperature structure was basically isostructural, there were large thermal parameters for some of the carbon atoms and geometric distortions of the C–C framework. At least one other orientation of the C_{80} cage was clearly present. The scandium atoms were distributed over the interior in at least 16 different sites, the largest with 0.15 occupancy and the smallest with 0.05 occupancy. Interestingly, the central N atom of the Sc_3N unit was one of the few well-behaved atoms. It thus appears that there is a reversible ordering of the ball and its contents as the crystal is cooled. Such orientational ordering is well known for C_{60} and has been observed to occur as a distinct phase change at the transition temperature of 168 K in $2C_{60}\cdot 3CS_2$.[19] Further experiments on this system are planned in order to describe the phase transitions involved.

Discussion

The TNT approach has been successfully utilized to prepare and purify the new endohedral $Lu_3N@C_{80}$. Comparison of the structures of $Lu_3N@C_{80}$ and $Sc_3N@C_{80}$ reveals that the fullerene cage retains the same size even when it accommodates the larger lutetium atoms. The Lu_3N portion, like the corresponding Sc_3N portion, is nearly planar, and the Lu–N distances are similar to the Sc–N distances. Consequently, the

  0947-6539/02/0819-4533 $ 20.00+.50/0

C_{80} cage constrains both metals, despite their expected differences, to very similar geometries. However, there is significant disorder in the positions of the metal ions within the cage even at 90 K. Theoretical calculations have shown that there is little energetic difference between a variety of selected locations of the Sc_3N unit within $Sc_3N@C_{80}$.[8, 17] Consequently, it is not surprising to find the Lu_3N and Sc_3N units occupying several sites within the C_{80} cage. Indeed given the high symmetry of the I_h C_{80} cage and the small distortions of the cage that the metal atoms produce, it is surprising that the interior contents of these endohedral are as ordered as they are, particularly for $Sc_3N@C_{80}$. For a striking comparison, note that the two erbium atoms in isomer I of $Er_2@C_{82}$ are distributed over 23 sites in crystalline $Er_2@C_{82}\cdot Co^{II}(OEP)\cdot 1.4(C_6H_6)\cdot 0.3(CHCl_3)$.[20]

Previous structural studies of endohedral complexes, including $Sc_3N@C_{80}$,[5] $ErSc_2N@C_{80}$,[13] $Sc_3N@C_{78}$,[11] $Er_2@C_{82}$,[19] and $Kr@C_{60}$,[21] have used co-crystallization with a metalloporphyrin as a method of obtaining suitable crystals with sufficient ordering of the fullerene cage to produce informative structural information.[22] However, only in the cases of $Er_2@C_{82}$[19] and $Kr@C_{60}$[20] did the fullerene cages adopt a single orientation that allowed individual refinement of the cage carbon atoms. The serendipitous discovery that $Lu_3N@C_{80}$ and $Sc_3N@C_{80}$ crystallize from *o*-xylene in a form that involves only one fullerene cage orientation makes this procedure the preferred method of crystallizing endohedral fullerenes of the $M_nSc_{3-n}N@C_{80}$ family.

Experimental Section

Formation of $Lu_3N@C_{80}\cdot 5$(*o*-xylene): Graphite rods (0.5 cm diameter, 15.5 cm length) were core-drilled and subsequently packed with cobalt oxide (180 mg) in a mixture of of graphite powder (1.0 g), Lu_2O_3 (2.5 g) per 3.2 g of hollowed graphite rod. These rods were then vaporized in a Krätschmer–Huffman-type fullerene generator under dynamic flow of He (1250 mL min^{-1}) and N_2 (22 mL min^{-1}) to obtain samples that contained $Lu_3N@C_{80}$. The resulting soot from this process was extracted with boiling *o*-xylene to obtain the initial endohedral extract. A NI-DCI mass spectrum of a typical extract solution is shown in Figure 1.

Separation of $Lu_3N@C_{80}\cdot 5$(*o*-xylene): The purification of $Lu_3N@C_{80}$ utilized a two-stage HPLC procedure. The initial scandium and lutetium fullerene extracts in *o*-xylene were injected directly into a pentabromobenzyl (PBB) column (Phenomenex, 10×250 mm) for a first-pass preparative cleanup. The objective of this first PBB pass was to remove the dominant C_{60} and C_{70} empty-cage fullerenes and obtain an enriched HPLC fraction of metallofullerenes (both classical and TNT-based). By using a flow rate of 6 mL min^{-1} of xylene, the TNT metallofullerene-enriched fraction eluted and was collected from 40–45 minutes. The second stage of the purificationc scheme involved the injection of the enriched PBB fraction *o*-xylene into a BuckyPrep column (Phenomenex, 10×250 mm). The dominant peak for these series of BuckyPrep injections was always the TNT metallofullerene of interest. A smaller HPLC peaks resulted from the classical metallofullerene $Lu_3N@C_{80}$ as well as empty-cage fullerenes C_{84}–C_{90}. Continuous injection and re-injection of the dominant peak eventually resulted in a single, sharp homogeneous peak (Figure 2). To ascertain the purity of these collected fractions, mass spectra characterization was necessary. The final HPLC traces as well as their corresponding mass spectral data (Kratos MALDI-TOF) are shown in Figure 2. Similar techniques were employed in the preparation and separation of $Sc_3N@C_{80}$.

Crystal growth for $Lu_3N@C_{80}\cdot 5$(*o*-xylene) and $Sc_3N@C_{80}\cdot 5$(*o*-xylene): Crystals of $Lu_3N@C_{80}\cdot 5$(*o*-xylene) and $Sc_3N@C_{80}\cdot 5$(*o*-xylene) suitable for X-ray crystallography were obtained by dissolving each compound in hot *o*-xylene and allowing the solution to cool slowly.

X-ray crystallography and data collection: The black crystals were removed from the glass tubes in which they were grown together with a small amount of mother liquor and immediately coated with a hydrocarbon oil on the microscope slide. Suitable crystals were mounted on glass fibers with silicone grease and placed in the cold stream of a Bruker SMART CCD with graphite-monochromated $Mo_{K\alpha}$ radiation at 90(2) K. Check reflections were stable throughout data collection. Crystal data are given in Table 1.

The structures were solved by direct methods and refined using all data (based on F^2) using the software of SHELXTL 5.1. Hydrogen atoms were added geometrically to the *o*-xylene carbon atoms and refined with a riding model.

CCDC-184939 and CCDC-184940 contain the supplementary crystallographic data for this paper. These data can be obtained free of charge via www.ccdc.cam.ac.uk/conts/retrieving.html (or from the Cambridge Crystallographic Data Centre, 12 Union Road, Cambridge CB2 1EZ, UK; fax: (+44) 1223-336-033; or e-mail: deposit@ccdc.cam.ac.uk).

Acknowledgement

We thank the US National Science Foundation (Grant CHE 0070291 to A.L.B.) for support. The Bruker SMART 1000 diffractometer was funded in part by NSF Instrumentation grant CHE-9808259.

[1] J. R. Heath, S. C. O'Brien, Q. Zhang, Y. Liu, R. F. Curl, H. W. Kroto, F. K. Tittel, R. E. Smalley, *J. Am. Chem. Soc.* **1985**, *107*, 7779.
[2] H. Shinohora in *Fullerenes: Chemistry, Physics, and Technology* (Eds.: K. M. Kadish, R. S. Ruoff) Wiley, New York, **2000**, p. 357.
[3] S. Nagase, K. Kobayashi, T. Akasaka, T. Wakahara in *Fullerenes: Chemistry, Physics, and Technology* (Eds.: K. M. Kadish, R. S. Ruoff), Wiley, New York, **2000**, p. 395.
[4] H. Shinohara, *Rep. Prog. Phys.* **2000**, *63*, 843.
[5] S. Stevenson, G. Rice, T. Glass, K. Harich, F. Cromer, M. R. Jordan, J. Craft, E. Hadju, R. Bible, M. M. Olmstead, K. Maitra, A. J. Fisher, A. L. Balch, H. C. Dorn, *Nature* **1999**, *401*, 55.
[6] H. C. Dorn, S Stevenson, J. Craft, F. Cromer, J. Duchamp, G Rice, T Glass, K Harich, P. W. Fowler, T. Heine, E. Hajdu, R. Bible, M. M. Olmstead, K. Maitra, A. J. Fisher, A. L. Balch, *Proceedings of the IWEPNM2000 Conference*, Kirchberg/Tyrol (Austria), March 4–10, **2000**, American Institute of Physics, in press.
[7] P. W. Fowler, D. E. Manoloupoulos, *An Atlas of Fullerenes*, Oxford University Press, Oxford, **1995**, p. 254.
[8] J. M. Campanera, C. Bo, M. M. Olmstead, A. L. Balch, J. M. Poblet, unpublished results.
[9] E. B. Iezzi, J. C. Duchamp, K. Harich, T. E. Glass, H. M. Lee, M. M. Olmstead, A. L. Balch, H. C. Dorn, *J. Am. Chem. Soc.* **2002**, *124*, 524.
[10] H. M. Lee, M. M. Olmstead, E. Iezzi, J. C. Duchamp, H. C. Dorn, A. L. Balch, *J. Am. Chem. Soc.* **2002**, *124*, 3494.
[11] M. M. Olmstead, A. de Bettencourt-Dias, J. C. Duchamp, S. Stevenson, D. Marciu, H. C. Dorn, A. L. Balch, *Angew. Chem.* **2001**, *113*, 1263; *Angew. Chem. Int. Ed.* **2001**, *40*, 1223.
[12] S. Stevenson, P. W. Fowler, T. Heine, J. C. Duchamp, G. Rice, T. Glass, K. Harish, E. Hajdu, R. Bible, H. C. Dorn, *Nature* **2000**, *408*, 427.
[13] M. M. Olmstead, A. de Bettencourt-Dias, J. C. Duchamp, S. Stevenson, H. C. Dorn, A. L. Balch, *J. Am. Chem. Soc.* **2000**, *122*, 12220.
[14] R. M. Macfarlane, D. S. Bethune, S. Stevenson, H. C. Dorn, *Chem. Phys. Lett.*, **2001**, *343*, 229.
[15] I. N. Ioffe, A. S. Ievlev, O. V. Boltalina, L. N. Sidorov, H. C. Dorn, S. Stevenson, G. Rice, *Int. J. Mass Spectrom.* **2002**, *213*, 183.
[16] F. A. Cotton, G. Wilkinson, *Advanced Inorganic Chemistry*, 4th ed., Wiley, New York, p. 982.
[17] K. Kobayashi, Y. Sano, S. Nagase, *J. Comput. Chem.* **2001**, *22*, 1353.
[18] R. C. Haddon, K. Raghavachari in *Buckminsterfullerenes* (Eds. W. E. Billups, M. A. Ciufolini), VCH, Weinehim (Germany), **1993**, Chapter 7.

  0947-6539/02/0819-4534 $ 20.00+.50/0

[19] M. M. Olmstead, F. Jiang, A. L. Balch, *Chem. Commun.* **2000**, 483.
[20] M. M. Olmstead, A. de Bettercourt-Dias, S. Stevenson, H. C. Dorn, A. L. Balch, *J. Am. Chem. Soc.* **2002**, *124*, 4172.
[21] H. M. Lee, M. M. Olmstead, T. Suetsuna, H. Shimotani, N. Dragoe, R. J. Cross, K. Kitazawa, A. L. Balch, *Chem. Commun.* **2002**, 1352.
[22] M. M. Olmstead, D. A. Costa, K. Maitra, B. C. Noll, S. L. Phillips, P. M. Van Calcar, A. L. Balch, *J. Am. Chem. Soc.* **1999**, *121*, 7090.

Received: May 6, 2002 [F4070]

  0947-6539/02/0819-4535 $ 20.00+.50/0